

Deep learning AI and Restriction Spectrum Imaging for patient-level detection of clinically significant prostate cancer on MRI

Yuze Song^{1,2}, Mariluz Rojo Domingo¹, Christopher C Conlin³, Deondre D Do^{1,4}, Madison T Baxter¹, Anna Dornisch¹, George Xu¹, Aditya Bagrodia⁵, Tristan Barrett³, Mukesh Harisinghani⁶, Gary Hollenberg⁷, Sophia Kamran⁸, Christopher J Kane⁵, Dimitri A Kessler^{9,10}, Joshua Kuperman¹, Kanglung Lee⁹, Michael A Liss⁵, Daniel JA Margolis¹¹, Paul M Murphy³, Nabih Nakrour⁶, Truong Ngyuen², Thomas L Osinski¹², Rebecca Rakow-penner³, Shoumik Roychowdhury¹³, Ahmed S Shabik¹⁴, Shaun Trecarten¹⁵, Natasha Wehrli¹¹, Eric P Weinberg⁷, Sean A Woolen¹⁶, Anders M Dale^{3,17,18}, Tyler M Seibert^{1,3,4,5}

¹Department of Radiation Medicine, University of California San Diego, La Jolla, CA, USA

²Department of Electrical and Computer Engineering, University of California San Diego, La Jolla, CA, USA

³Department of Radiology, University of California San Diego, La Jolla, CA, USA

⁴Department of Bioengineering, University of California San Diego, La Jolla, CA, USA

⁵Department of Urology, University of California San Diego, La Jolla, CA, USA

⁶Department of Radiology, Massachusetts General Hospital, Boston, MA, USA

⁷Department of Clinical Imaging Sciences, University of Rochester Medical Center, Rochester, NY, USA

⁸Department of Radiation Oncology, Massachusetts General Hospital, Boston, MA, USA

⁹Department of Radiology, University of Cambridge, Cambridge, United Kingdom

¹⁰Artificial Intelligence in Medicine Lab (BCN-AIM), Facultat de Matemàtiques i Informàtica, Universitat de Barcelona, Barcelona, Spain

¹¹Department of Radiology, Cornell University, Ithaca, NY, USA

¹²Department of Urology, University of Rochester Medical Center, Rochester, NY, USA

¹³Department of Electrical Engineering and Computer Sciences, University of Berkeley, Berkeley, CA, USA

¹⁴Department of Pathology, University of California San Diego, La Jolla, CA, USA

¹⁵Department of Urology, University of Texas Health Sciences Center San Antonio, San Antonio, TX, USA

¹⁶Department of Radiology and Biomedical Imaging, University of California San Francisco, San Francisco, CA, USA

¹⁷Department of Neurosciences, University of California San Diego, La Jolla, CA, USA

¹⁸Harold Gill Data Science Institute, University of California San Diego, La Jolla, CA, USA

NOTE: This preprint reports new research that has not been certified by peer review and should not be used to guide clinical practice.

Abstract

Background:

The Prostate Imaging Reporting & Data System (PI-RADS), based on multiparametric MRI (mpMRI), is widely used for the detection of clinically significant prostate cancer (csPCa, Gleason Grade Group (GG \geq 2)). However, its diagnostic accuracy can be impacted by variability in interpretation. Restriction Spectrum Imaging (RSI), an advanced diffusion-weighted technique, offers a standardized, quantitative approach for detecting csPCa, potentially enhancing diagnostic consistency and performing comparably to expert-level assessments.

Purpose:

To evaluate whether combining maximum RSI-derived restriction scores (RSIrs-max) with deep learning (DL) models can enhance patient-level detection of csPCa compared to using PI-RADS or RSIrs-max alone.

Materials and Methods:

Data from 1,892 patients across seven institutions were analyzed, selected based on MRI results and biopsy-confirmed diagnoses. Two deep learning architectures, 3D-DenseNet and 3D-DenseNet+RSI (incorporating RSIrs-max), were developed and trained using biparametric MRI (bpMRI) and RSI data across two data splits. Model performance was compared using the area under the receiver operating characteristic curve (AUC) for patient-level csPCa detection, using PI-RADS performance for clinical reference.

Results:

Neither RSIrs-max nor the best DL model combined with RSIrs-max significantly outperformed PI-RADS interpretation by expert radiologists. However, when combined with PI-RADS, both approaches significantly improved patient-level csPCa detection, with AUCs of 0.79 (95% CI: 0.74-0.83; $P=.005$) for combination of RSIrs-max with PI-RADS and 0.81 (95% CI: 0.76-0.85; $P<.001$) for combination of best DL model with PI-RADS, compared to 0.73 (95% CI: 0.68-0.78) for PI-RADS alone.

Conclusion:

Both RSIrs-max and DL models demonstrate comparable performance to PI-RADS alone. Integrating either model with PI-RADS significantly enhances patient-level detection of csPCa compared to using PI-RADS alone.

Summary Statement:

RSIrs-max and deep learning models match the performance of expert PI-RADS in patient-level csPCa detection and combining either with PI-RADS yields a significant improvement over PI-RADS alone.

Key Points:

- In a study of 1,892 patients from seven institutions undergoing MRI and biopsy for prostate cancer, RSIrs-max and the DL model (AUC, 0.75 ($P=.59$) and 0.78 ($P=.09$)) performed comparably to expert-level PI-RADS scores (AUC, 0.73).
- Including prostate auto-segmentation improved the DL model (AUC, 0.68 ($P=.01$) vs 0.72 ($P=.60$)).
- Combining RSIrs-max or the DL model (AUC, 0.79 ($P=.005$) and 0.81 ($P <.001$)) with PI-RADS statistically significantly outperformed PI-RADS alone (AUC, 0.73).

Introduction

Multiparametric magnetic resonance imaging (mpMRI) plays a key role in the early diagnosis of prostate cancer, as recommended by the European Association of Urology (EAU) and National Comprehensive Cancer Network (NCCN) guidelines¹. mpMRI has been shown to reduce unnecessary biopsies and improve the detection of clinically significant prostate cancer (csPCa, grade group (GG) ≥ 2)¹⁻⁴. The Prostate Imaging Reporting & Data System (PI-RADS v2.1) was developed to provide a standardized approach for interpreting mpMRI. However, interpretation can still vary based on the reader's experience and training. As the incidence of prostate cancer is expected to increase in the coming years, there may be challenges in meeting demand with the current supply of trained experts⁶. An accurate, supportive tool for interpreting prostate MRI could facilitate standardization and address variability in clinical practice⁷.

Restriction Spectrum Imaging (RSI) is an advanced technique for diffusion-weighted imaging (DWI) that measures signal from four distinct tissue compartments: restricted intracellular water (RSI-C₁), hindered extracellular water (RSI-C₂), freely diffusing water (RSI-C₃), and vascular flow (RSI-C₄)^{1,2}. RSI restriction score (RSIs) is a quantitative biomarker based on RSI that has been shown to be superior to Apparent Diffusion Coefficient (ADC) for detection of csPCa³⁻⁶. Moreover, when maximum RSIs (RSIs-max) is combined with PI-RADS, the performance for patient-level detection of csPCa has been shown to be superior to either alone^{4,6}.

PI-RADS relies predominantly on the T_2 -weighted imaging (T2w) and DWI components of mpMRI, collectively called biparametric MRI (bpMRI)⁷. There is interest in moving toward bpMRI for many patients, as bpMRI avoids the risks and costs associated with intravenous contrast⁸⁻¹¹. Deep learning artificial intelligence (AI) models have been developed based on bpMRI for objective and reproducible detection and localization of csPCa, with results matching those of expert radiologists¹²⁻¹⁶.

As both RSI and deep-learning AI models been shown to be accurate and useful for methods, we investigated whether combining the two would improve the automated patient-level detection of csPCa.

Materials and Methods

Study Population

The data for this study comes from seven imaging centers participating in the Quantitative Prostate Imaging Consortium (QPIC): the Center for Translational Imaging and Precision Medicine at the University of California San Diego (CTIPM), UC San Diego Health (UCSD), University of California San Francisco (UCSF), Harvard University affiliated Massachusetts General Hospital (MGH), University of Rochester Medical Center (URMC), University of Texas Health Sciences Center San Antonio (UTHSCSA), and University of Cambridge (Cambridge)⁶. The study was approved by each center's institutional review

board (IRB). At UTHSCSA and Cambridge, the data were collected prospectively as part of related projects with written informed consent. At the other centers, the data were collected retrospectively, and a waiver of consent was approved by the respective IRBs for secondary use of routine clinical data. Individuals were included if aged ≥ 18 years and underwent prostate MRI for suspected PCa or active surveillance between January 2016 and March 2024. They were excluded if they had prior treatment of PCa or if there was no available biopsy result from within 6 months of a positive MRI scan (PI-RADS ≥ 3). Patients with metallic implants were also excluded to avoid metal-induced imaging artifacts. The diagnosis of csPCa was confirmed on biopsy histopathology as per standard-of-care practice at each center. These data have been previously analyzed for performance of RSIs-max^{4,6,17} (Figure 1).

Data acquisition and processing

The processing for RSI data included correction for background noise, eddy currents, and gradient nonlinearities¹⁸⁻²⁰. Correction for distortion caused by B_0 inhomogeneity was applied to data acquired at CTIPM²¹. ADC, DWI and RSI data were resampled to the same image resolution as the T2w data. Automated prostate contours were obtained using an FDA-cleared commercial product (OnQ Prostate, CorTechs.ai, San Diego, CA).

For RSI data, the signal intensity for each b-value was modeled as a linear combination of exponential decays representing four diffusion compartments (RSI-C₁, RSI-C₂, RSI-C₃ and RSI-C₄), each with a diffusion coefficient determined empirically in previous work². The RSIs biomarker is the intensity value of the RSI-C₁ signal at a given voxel normalized by median T₂-weighted signal in the prostate. RSIs-max is the maximum RSIs value within a given patient's prostate. Additional details regarding the RSI modeling are provided in Supplementary Materials.

Model

RSIs-max-only and PI-RADS-only were previously analyzed for performance of patient-level csPCa detection using univariable logistic regression⁶. Here, we compare the performance of deep learning models to those previously described logistic regression models. 3D-DenseNet²¹ and 3D-DenseNet+RSI, both 3D densely connected convolutional networks, were trained to get the probability of csPCa with different modalities. The details of the models are illustrated in Figure 2.

The loss function used to supervise the two models is the Cross Entropy Loss ($LOSS_{CE}$):

$$LOSS_{CE} = -\frac{1}{N} \left[\sum_{j=1}^N [t_j \log(p_j) + (1 - t_j) \log(1 - p_j)] \right] \quad (1)$$

In the equation (1), N is the number of data points. t_j refers to the ground truth value. If the patient has a csPCa, then t_j is 1. p_j is the SoftMax probability for the i^{th} data point.

We also use either RSIs-max or output probabilities of the AI models, along with PI-RADS, as inputs to a multivariable logistic regression model for comparison with either alone.

Implementation Details

We employed two different data splits for this study (Figure 1). Data Split 1 was used to test all models and was chosen to facilitate direct comparison with a previous study⁶, which also used Data Split 1; Data Split 2 allocated a larger and more diverse dataset for training because deep learning models' performance typically improves substantially when trained on heterogeneous data. Data Split 2 was used for testing the model with RSIs-max-only input; the PI-RADS-only input; the best-performing deep learning model; the combination of RSIs-max and PI-RADS; and the combination of the output probability from the best-performing deep learning model and PI-RADS from analysis of Data Split 1. We also divided and tested the data for both splits based on GG.

Data Split 1 was described previously^{6,17}. Scans collected with the RSI acquisition protocol and the same scanner model (GE Healthcare Discovery MR750) were used for training (n=554). The remaining protocols were used for the testing dataset (n=664) with patients who were biopsy-naïve at the time of the MRI scan and received a biopsy following the MR acquisition. The validation dataset (n=628) is from the rest of the patients that are not included in either training or testing data of Data Split 1 (Table 1).

The training set for Data Split 2 (n=898) includes data from different RSI protocols and collected from two centers (UCSD CTIPM and URMC). Data from UCSD CTIPM were collected using GE Healthcare Discovery MR750 and GE Healthcare Signa Premier scanners. Data from URMC were collected from SIEMENS Magnetom Skyra scanners. The testing dataset (n=384) is from the remaining patients of all other cohorts who were biopsy-naïve at the time of the MRI scan and received a biopsy following the MR acquisition. The validation dataset (n=564) for Data Split 2 is from the rest of the patients that are not included in either training or testing data of Data Split 2 (Table 1). Both testing and validation datasets are external to the training dataset.

Two univariable logistic regression models (RSIs-max or PI-RADS as input, respectively) and two multi-variable logistic regression models (combination of RSIs-max or output probability of the best performing AI model with PI-RADS as inputs, respectively) were implemented using MATLAB.

The RSI-C₁ and RSI-C₂ components from RSI data, T2w, ADC and high b-value DWI (high-b DWI) were included as the 3D-data for the input of the corresponding model. The preprocessing and augmentation of the input image data is described in Supplementary Materials. The following models were evaluated: Model 1: PI-RADS; Model 2: RSIs-max; Model 3 (bpMRI): T2w, ADC, high-b DWI; Model 4 (bpMRI-seg): T2w with automated prostate segmentation applied as a binary mask (T2w-seg), ADC-seg, high-b DWI-seg; Model 5: bpMRI-seg, RSIs-max; Model 6 (bpMRI-seg, RSI-seg, RSIs-max): bpMRI-seg, RSI-C₁-seg, RSI-C₂-seg, RSIs-max; Model 7: RSIs-max, PI-RADS and Model 8: bpMRI-seg, RSI-seg, RSIs-max, PI-RADS (Table 2 and Table 3). For all inputs labeled with “-seg”,

the automated prostate segmentation was applied to the 3D data as a binary mask through element-wise multiplication.

All models, preprocessing, and data augmentation were implemented using the PyTorch toolbox and MONAI²². The training details is described in Supplementary Materials.

Statistical analysis

The precise location and extent of csPCa in each patient's prostate are generally unknown, and targeted biopsy can have MRI-to-ultrasound registration or needle placement errors. Many cancers are also detected through systematic biopsy. We therefore focus on patient-level csPCa detection, a more reliable approach that addresses the key clinical question of whether to recommend an invasive biopsy. The performance for patient-level detection was assessed by the Area Under the Curve of the Receiver Operating Characteristic curve (AUC). For the two data splits, we made statistical comparisons via 10,000-bootstrapping samples to calculate 95% confidence intervals and *P* for the difference between the performance of the models and PI-RADS²³. The primary analysis was for detection of GG \geq 2 (csPCa) versus GG=1 and Benign (non-csPCa), for which we determined the statistical significance through a two-sided $\alpha=0.05$. Secondary subgroup analyses evaluated the results per GG. For Data Split 2, we repeated the above analyses for PI-RADS, RSIs-max, and the best performing deep learning model (based on median AUC for GG \geq 2) from the Data Split 1 analyses.

We trained a model with bpMRI and compared its performance with PI-RADS-only and RSIs-max-only univariable logistic regression models. To assess whether automated prostate contours could enhance performance, we also tested our model with bpMRI-seg input. Finally, we evaluated combining RSIs-max with bpMRI-seg to determine if RSIs-max improves performance over bpMRI-seg alone.

Codes used in developing the DL model are available on [GitHub](#).

Results

Data were acquired using 7 distinct acquisition protocols, 2 scanner vendors, 4 scanner models, and 17 MRI scanners (Table 1, Supplementary Table 2 and 3). 1,892 patients met the inclusion criteria (Figure 1). Occlusion sensitivity map²⁴ was generated for interpretation of the DL models (Figure 3 and 4).

Patient-level detection of csPCa for Data Split 1

Table 2 shows the AUC values of models with different 3D-inputs and testing groups for Data Split 1. We tested our model on 4 groups, none of which were used during training. Group A (n=664) consists of patients that were biopsy-naïve at time of MRI and then either had a biopsy to determine cPCa status or were presumed non-csPCa based on low clinical suspicion. Group B (n=500) is the subset of Group A consisting of patients with GG2 csPCa or non-csPCa (i.e., excluding GG \geq 3). Group C (n=409) is the subset of Group A consisting

of patients with GG3 csPCa or non-csPCa. Lastly, Group D (n=393) is the subset of Group A consisting of patients with high grade GG4-5 csPCa or non-csPCa (Table 1).

When an automated prostate segmentation was included (AUC, 0.72 (95% CI: 0.69-0.76; $P=.60$)), patient-level csPCa detection was comparable to PI-RADS (AUC, 0.74 (95% CI: 0.70-0.77)), whereas training the bpMRI model without the prostate segmentation (AUC, 0.68 (95% CI: 0.64-0.72; $P=.01$)) yielded worse performance than PI-RADS. The same pattern was observed for the subgroups based on GG.

Combining PI-RADS with either RSIs-max (AUC, 0.77 (95% CI: 0.73-0.81; $P=.01$)) or with the best deep learning model (Model 6) (AUC, 0.78 (95% CI: 0.74-0.81; $P<.001$)) yielded significantly improved patient-level csPCa detection compared to PI-RADS alone (AUC, 0.74 (95% CI: 0.70-0.77)).

The quantitative biomarker RSIs-max performed comparably in comparison of PI-RADS ($P=.49$) and the bpMRI-seg deep learning AI model ($P=.85$). Combining RSIs-max with the deep learning bpMRI-seg model did not result in a statistically significant improvement in csPCa detection with PI-RADS, with ($P=.87$) or without ($P=.49$) the 3D volumes from RSI-C₁ and RSI-C₂. This suggests that a straightforward, interpretable biomarker (RSIs-max) derived from approximately two minutes of RSI acquisition may capture most of the valuable information provided by bpMRI. However, when PI-RADS was combined with RSIs-max ($P=.01$), performance was significantly superior to PI-RADS alone. Likewise, combining PI-RADS with the best deep learning model ($P<.001$) also improved performance beyond PI-RADS alone.

Patient-level detection of csPCa for Data Split 2

The best-performing AI model in Data Split 1 analyses (based on median AUC) was Model 6. We therefore calculated and compared AUC values of Models 1, 2 and 6 within Data Split 2 (Table 3). Group E (n=384) is the full testing dataset for Data Split 2, consisting of either the patients that are biopsy-naïve at time of MRI with a biopsy confirmed diagnosis or are non-csPCa. Group F (n=255) is a subset of Group E consisting of patients with GG2 csPCa and non-csPCa. Group G (n=228) is another subset of Group E consisting of patients with GG3 csPCa and non-csPCa. Lastly, Group H (n=211) is also another subset of Group E consisting of patients with GG4-5 csPCa and non-csPCa.

RSIs-max (AUC, 0.75 (95% CI: 0.70-0.80; $P=.59$)) and the AI model (Model 6) (AUC, 0.78 (95% CI: 0.73-0.83; $P=.09$)) had higher point estimates for AUC than PI-RADS (AUC, 0.73 (95% CI: 0.68-0.78)) in Data Split 2, but there was no statistically significant difference between any of these models. Interestingly, though, while the AUC for PI-RADS was similar in the two data splits, the AI model performed better when trained on more diverse data: (AUC, 0.73 (95% CI: 0.69-0.77)) in the testing set for Data Split 1 and (AUC, 0.78 (95% CI: 0.73-0.83)) in the testing set for Data Split 2. Importantly, combining PI-RADS with either RSIs-max (AUC, 0.79 (95% CI: 0.74-0.83; $P=.005$)) or AI model (AUC, 0.81 (95% CI: 0.76-0.85; $P<.001$)) significantly outperformed PI-RADS alone.

Discussion

Previous work demonstrated the promising utility of RSIs-max as a quantitative imaging biomarker for csPCa^{2-4,6,25}. In this study, we explored deep learning AI as an alternative or complementary approach for reproducible, objective interpretation of prostate MRI. We observed comparable performance in csPCa detection using PI-RADS, a bpMRI AI model, and RSIs-max. While training AI models with bpMRI and RSI data (RSIs-max alone or with full RSI volumes) showed a numerical improvement in detection, it was not statistically significant. However, combining PI-RADS with either the best AI model (Model 6) or RSIs-max significantly enhanced detection performance compared to PI-RADS alone. Thus, RSIs-max provides rapid, quantitative, standardized data to support radiologist interpretation and could augment PI-RADS scoring.

An advantage of a bpMRI AI tool over RSIs-max is that it may be applicable to datasets lacking DWI compatible with calculation of RSIs-max. The deep learning model does not rely on the radiologist's expertise and offers results comparable to PI-RADS, which could make it a useful tool in helping less experienced prostate radiologists perform more accurately, to address the growing shortage of subspecialist expert radiologists²⁶.

It is worth noting that the bpMRI AI model achieved better performance when incorporating an automated segmentation of the prostate. This result suggests it can be more efficient and accurate to train a model with known prior anatomical information.

RSIs-max, initially trained on a small cohort of 46 patients from a single institution, demonstrates strong generalization due to its biophysical basis and alignment with cancer cell morphology^{1,2,6,17,27}. Conversely, AI models, are known to benefit from larger and more diverse training datasets. We found that expanding the training data (i.e., moving from Data Split 1 to Data Split 2) improved the AI model performance slightly from (AUC, 0.73 (95% CI: 0.69-0.77)) in Data Split 1 to (AUC, 0.78 (95% CI: 0.73-0.83)) in Data Split 2. These are different datasets, so the AUCs are not directly comparable, but neither PI-RADS nor RSIs-max saw a similar boost in performance between the two data splits. With larger datasets, combining AI and RSI may even achieve superior performance.

The combination of RSIs-max or the best deep learning model (Model 6) with PI-RADS achieved statistically significantly better results than PI-RADS alone. This finding suggests that both RSIs-max and the deep learning model can serve as complementary tools to PI-RADS for detection of csPCa.

The performance of our models are concordant with other recent studies of AI for prostate MRI that also showed patient-level csPCa detection comparable to PI-RADS^{12,28}. For example, in the PI-CAI challenge, an AI model was developed as a single combination of the 5 best performing models (among 293 submitted for the challenge) and performed similarly to radiologists¹². Of note, beyond imaging data, the PI-CAI model also included age,

prostate-specific antigen (PSA) level, prostate volume, and scanner name. Another recent study described two models developed for patient-level detection: one with only imaging data, and another that combined imaging with PSA and PSA density²⁸. Performance of AI models is best assessed in external validation datasets. Saha et al. (PI-CAI study) tested their model in data from 1,000 patients from four centers, all using Siemens Healthineers scanners (mainly Siemens Skyra)¹². Cai et al. tested their model in data from 604 patients from 3 sites of a single academic institution using 2 scanner vendors (Siemens Healthineers and GE Healthcare) and an external dataset²⁸. Our Data Split 1 had 664 patients in the testing set from 6 imaging centers and 2 scanner vendors (Siemens Healthineers and GE Healthcare). Data Split 2 had 384 patients in the testing set from 5 imaging centers and the same 2 scanner vendors (Siemens Healthineers and GE Healthcare).

Limitations of our study include those typical for prostate MRI: (1) biopsy is an imperfect gold standard due to possibility of missing csPCa, even when targeting with MRI, and (2) individuals with hip implants were excluded because of known potential to cause severe artifacts on MRI. Larger datasets could facilitate improved AI training, smaller confidence intervals, and increased statistical power to detect differences between models. To our knowledge, though, this is the largest study to date to combine AI and an advanced MRI biomarker for prostate cancer. Finally, we evaluated only one type of deep learning model here; future research will include additional AI architectures.

Conclusions

Deep learning bpMRI and the RSIRs-max imaging biomarker achieve performance comparable to expert radiologists for detecting csPCa. Combining PI-RADS with RSIRs-max or an AI model outperformed PI-RADS alone, suggesting that both could serve as valuable complements to human expertise. Larger datasets may reveal advantages to integrating RSI in AI.

Reference

1. Brunsing RL, Schenker-Ahmed NM, White NS, et al. Restriction spectrum imaging: An evolving imaging biomarker in prostate MRI: Prostate MRI with Restriction Spectrum Imaging: A Review. *J Magn Reson Imaging*. 2017;45(2):323-336. doi:10.1002/jmri.25419
2. Conlin CC, Feng CH, Rodriguez-Soto AE, et al. Improved Characterization of Diffusion in Normal and Cancerous Prostate Tissue Through Optimization of Multicompartmental Signal Models. *J Magn Reson Imaging*. 2021;53(2):628-639. doi:10.1002/jmri.27393
3. Feng CH, Conlin CC, Batra K, et al. Voxel-level Classification of Prostate Cancer on Magnetic Resonance Imaging: Improving Accuracy Using FOUR-COMPARTMENT Restriction Spectrum Imaging. *J Magn Reson Imaging*. 2021;54(3):975-984. doi:10.1002/jmri.27623
4. Zhong AY, Digma LA, Hussain T, et al. Automated patient-level prostate cancer detection with quantitative diffusion magnetic resonance imaging. *Eur Urol Open Sci*. 2023;47:20-28.
5. Lui AJ, Kallis K, Zhong AY, et al. ReIGNITE radiation therapy boost: a prospective, international study of radiation oncologists' accuracy in contouring prostate tumors for focal radiation therapy boost on conventional magnetic resonance imaging alone or with assistance of restriction spectrum imaging. *Int J Radiat Oncol Biol Phys*. 2023;117(5):1145-1152.
6. Rojo Domingo M, Do DD, Conlin CC, et al. Restriction Spectrum Imaging as a quantitative biomarker for prostate cancer with reliable positive predictive value. *medRxiv*. Published online 2024:2024-06.
7. Turkbey B, Rosenkrantz AB, Haider MA, et al. Prostate imaging reporting and data system version 2.1: 2019 update of prostate imaging reporting and data system version 2. *Eur Urol*. 2019;76(3):340-351.
8. Baxter MT, Conlin CC, Bagrodia A, et al. Advanced Restriction imaging and reconstruction Technology for Prostate MRI (ART-Pro): Study protocol for a multicenter, multinational trial evaluating biparametric MRI and advanced, quantitative diffusion MRI for detection of prostate cancer. *medRxiv*. Published online 2024:2024-08.
9. Asif A, Nathan A, Ng A, et al. Comparing biparametric to multiparametric MRI in the diagnosis of clinically significant prostate cancer in biopsy-naive men (PRIME): a prospective, international, multicentre, non-inferiority within-patient, diagnostic yield trial protocol. *BMJ Open*. 2023;13(4):e070280.
10. Eldred-Evans D, Burak P, Connor MJ, et al. Population-based prostate cancer screening with magnetic resonance imaging or ultrasonography: the IP1-PROSTAGRAM study. *JAMA Oncol*. 2021;7(3):395-402.
11. Schoots IG, Barentsz JO, Bittencourt LK, et al. PI-RADS Committee Position on MRI Without Contrast Medium in Biopsy-Naive Men With Suspected Prostate Cancer: Narrative Review. *Am J Roentgenol*. 2021;216(1):3-19. doi:10.2214/AJR.20.24268
12. Saha A, Bosma JS, Twilt JJ, et al. Artificial intelligence and radiologists in prostate cancer detection on MRI (PI-CAI): an international, paired, non-inferiority, confirmatory study. *Lancet Oncol*. Published online 2024. Accessed October 10, 2024. [https://www.thelancet.com/journals/lanonc/article/PIIS1470-2045\(24\)00220-1/abstract](https://www.thelancet.com/journals/lanonc/article/PIIS1470-2045(24)00220-1/abstract)
13. Yoo S, Gujrathi I, Haider MA, Khalvati F. Prostate cancer detection using deep convolutional neural networks. *Sci Rep*. 2019;9(1):19518.

14. Liu S, Zheng H, Feng Y, Li W. Prostate cancer diagnosis using deep learning with 3D multiparametric MRI. In: *Medical Imaging 2017: Computer-Aided Diagnosis*. Vol 10134. SPIE; 2017:581-584. Accessed October 10, 2024.
<https://www.spiedigitallibrary.org/conference-proceedings-of-spie/10134/1013428/Prostate-cancerdiagnosis-using-deep-learning-with-3D-multiparametric-MRI/10.1117/12.2277121.short>
15. De Vente C, Vos P, Hosseinzadeh M, Pluim J, Veta M. Deep learning regression for prostate cancer detection and grading in bi-parametric MRI. *IEEE Trans Biomed Eng*. 2020;68(2):374-383.
16. Arif M, Schoots IG, Castillo Tovar J, et al. Clinically significant prostate cancer detection and segmentation in low-risk patients using a convolutional neural network on multi-parametric MRI. *Eur Radiol*. 2020;30(12):6582-6592. doi:10.1007/s00330-020-07008-z
17. Do DD, Rojo Domingo M, Conlin CC, et al. Robustness of a Restriction Spectrum Imaging (RSI) quantitative MRI biomarker for prostate cancer: assessing for systematic bias due to age, race, ethnicity, prostate volume, medication use, or imaging acquisition parameters. *medRxiv*. Published online 2024:2024-09.
18. White NS, McDonald CR, Farid N, et al. Diffusion-weighted imaging in cancer: physical foundations and applications of restriction spectrum imaging. *Cancer Res*. 2014;74(17):4638-4652.
19. Zhuang J, Hrabe J, Kangarlu A, et al. Correction of eddy-current distortions in diffusion tensor images using the known directions and strengths of diffusion gradients. *J Magn Reson Imaging*. 2006;24(5):1188-1193. doi:10.1002/jmri.20727
20. Karunamuni RA, Kuperman J, Seibert TM, et al. Relationship between kurtosis and bi-exponential characterization of high b-value diffusion-weighted imaging: application to prostate cancer. *Acta Radiol*. 2018;59(12):1523-1529. doi:10.1177/0284185118770889
21. Huang G, Liu Z, Van Der Maaten L, Weinberger KQ. Densely connected convolutional networks. In: *Proceedings of the IEEE Conference on Computer Vision and Pattern Recognition*. ; 2017:4700-4708. Accessed October 10, 2024.
http://openaccess.thecvf.com/content_cvpr_2017/html/Huang_Densely_Connected_Convolutional_CVPR_2017_paper.html
22. Cardoso MJ, Li W, Brown R, et al. MONAI: An open-source framework for deep learning in healthcare. Published online November 4, 2022. Accessed October 10, 2024.
<http://arxiv.org/abs/2211.02701>
23. Efron B, Tibshirani R. Bootstrap methods for standard errors, confidence intervals, and other measures of statistical accuracy. *Stat Sci*. Published online 1986:54-75.
24. Zeiler MD. Visualizing and Understanding Convolutional Networks. In: *European Conference on Computer Vision/arXiv*. Vol 1311. ; 2014.
25. Domingo MR, Conlin CC, Karunamuni RA, et al. Utility of quantitative measurement of T2 using Restriction Spectrum Imaging for detection of clinically significant prostate cancer. *medRxiv*. Published online 2024:2024-03.
26. James ND, Tannock I, N'Dow J, et al. The Lancet Commission on prostate cancer: planning for the surge in cases. *The Lancet*. 2024;403(10437):1683-1722.
27. Zhong AY, Lui AJ, Kuznetsova S, et al. Clinical Impact of Contouring Variability for Prostate Cancer Tumor Boost. *Int J Radiat Oncol Biol Phys*. Published online 2024.

Accessed October 10, 2024.

<https://www.sciencedirect.com/science/article/pii/S0360301624007405>

28. Cai JC, Nakai H, Kuanar S, et al. Fully Automated Deep Learning Model to Detect Clinically Significant Prostate Cancer at MRI. Goh V, ed. *Radiology*. 2024;312(2):e232635.
doi:10.1148/radiol.232635

Figures

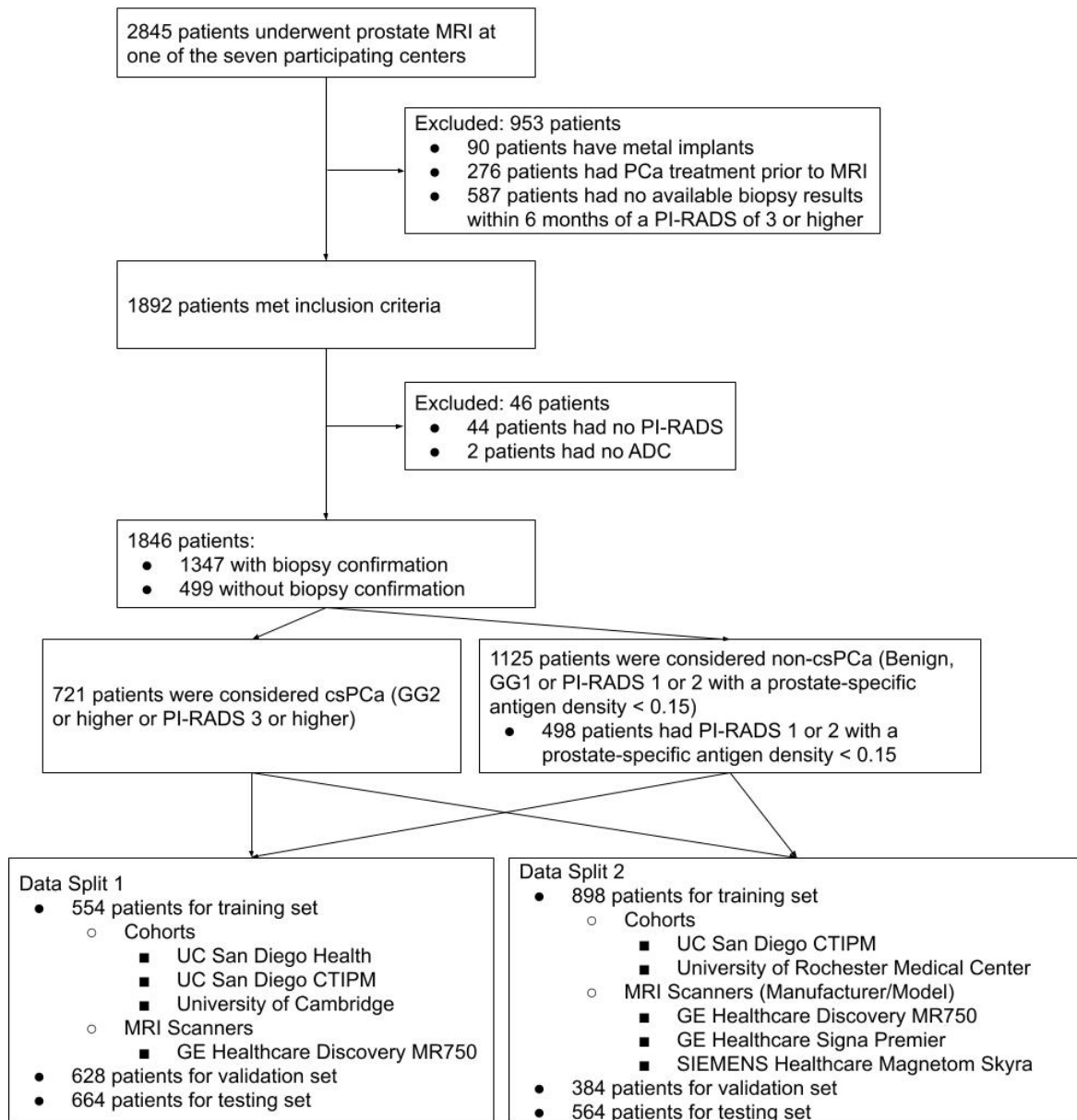
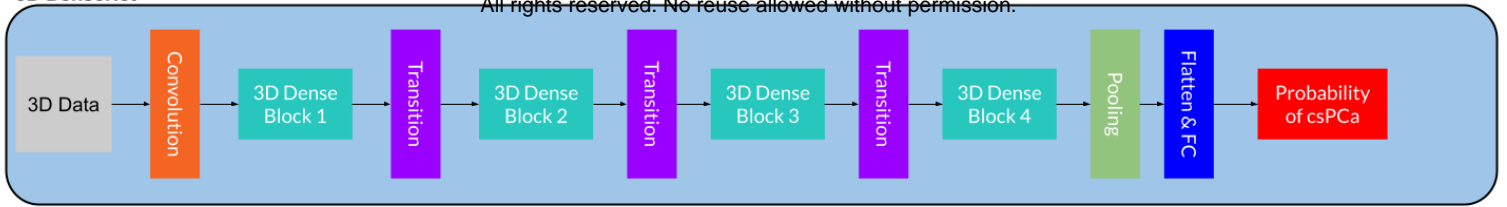


Figure 1. Flowchart shows inclusion and exclusion criteria and patient characteristics. PCa = Prostate Cancer. PI-RADS = Prostate Imaging Reporting and Data System. csPCa = Clinically Significant Prostate Cancer. ADC = Apparent Diffusion Coefficient. GG = Gleason Grade Group. UC = University of California. CTIPM = Center for Translational Imaging and Precision Medicine

3D DenseNet

All rights reserved. No reuse allowed without permission.



3D DenseNet+RSI

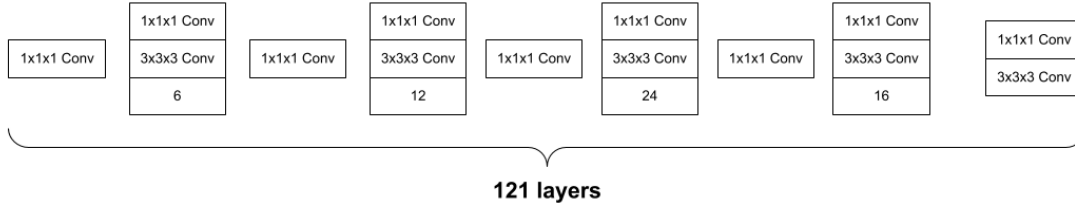
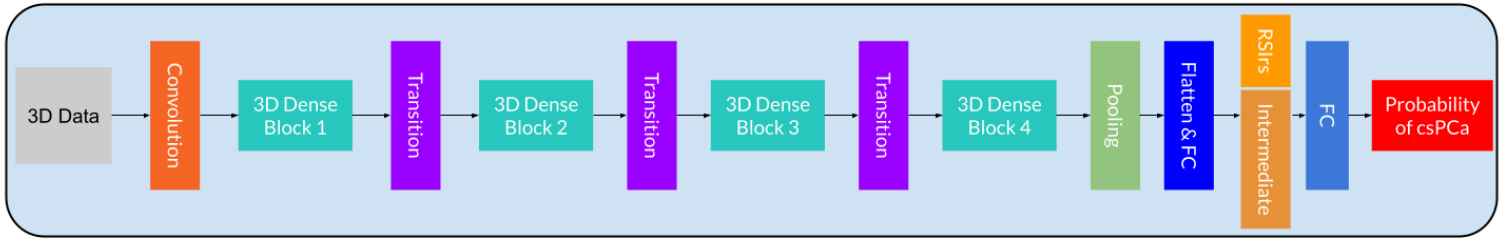


Figure 2. Overview of the experimental setup. 3D-Data are used as input of the 3D-DenseNet, followed by convolution layer, several 3D Dense Blocks and Transition layers, then after the Pooling layer and Flatten & Fully Connected (FC) layer, the 3D-DenseNet returns the final classification of csPCa or not. For 3D-DenseNet+RSI, the process before the Flatten & FC layer is the same, the remaining process is concatenating the intermediate output from the Flatten & FC layer with the RSIrs-max. Then, after going through another FC layer, the 3D-DenseNet+RSI gives the final output of probability of csPCa.

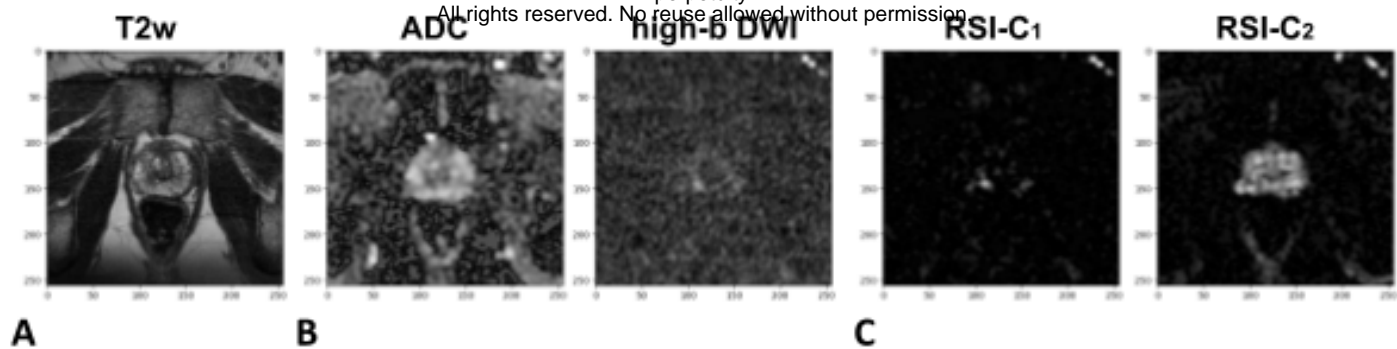


Figure 3. Male patient, age between 55 and 59, underwent MRI due to clinical suspicion of prostate cancer. The patient subsequently underwent prostatectomy and had Gleason Score 4 + 3 (GG 3) cancer at the right and left posterior near the apex of the prostate. He was included in both Data Split 1 and Data Split 2 test sets. The patient-level probability from Model 4 (AI bpMRI-seg) with Data Split 1 was 0.18, from Model 6 (AI bpMRI-seg + RSI-seg + RSIs-max) with Data Split 1 was 0.47, and from Model 6 with Data Split 2 was 0.51. The radiologists graded this examination as PI-RADS 4 for the lesion at the right peripheral zone at the posterior medial prostate within apex. **(A)** T_2 -weighted image (T2w, representative slice). **(B)** Apparent diffusion coefficient map (ADC, representative slice, left) and high-b diffusion-weighted image (high-b DWI, representative slice, right). **(C)** Intracellular (RSI-C₁, representative slice, left) and extracellular (RSI-C₂, representative slice, right) images.

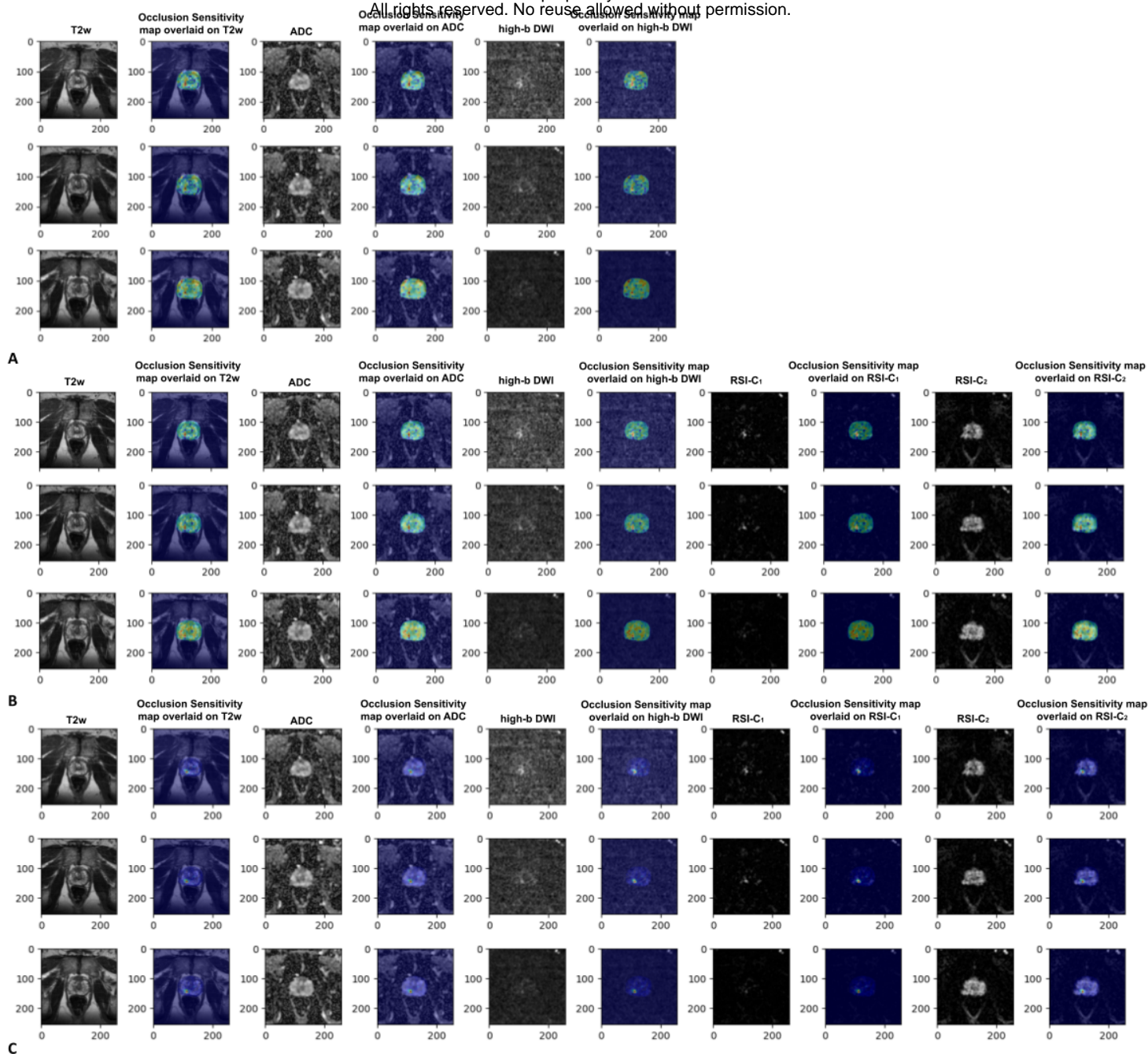


Figure 4. Scan from the same patient as Figure 3. **(A)** T2w, ADC, and high-b DWI images from left to right and with occlusion sensitivity maps from Model 4 (Data Split 1) overlaid at the right of each MRI images. **(B)** T2, ADC, high-b DWI, RSI-C₁, and RSI-C₂ images from left to right and with occlusion sensitivity maps from Model 6 (Data Split 1) overlaid at the right of each MRI images. **(C)** T2w, ADC, high-b DWI, RSI-C₁, and RSI-C₂ images from left to right with occlusion sensitivity maps from Model 6 (Data Split 2) overlaid at the right of each MRI images.

Tables

Characteristic	Training (Data Split 1)*	Validation (Data Split 1)	Testing (Data Split 1)	Training (Data Split 2)	Validation (Data Split 2)	Testing (Data Split 2)
No. of cases	554	628	664	898	564	384
Age (y)**	70 (64-75)	70 (65-75)	69 (64-74)	70 (64-74)	70 (65-75)	70 (64-75)
csPCa	192 (34.7)	184 (29.3)	345 (52.0)	376 (41.9)	116 (20.6)	229 (59.6)
non-csPCa	362 (65.3)	444 (70.7)	319 (48.0)	522 (58.1)	448 (79.4)	155 (40.4)
Cohorts						
UC San Diego Health	546 (98.6)	48 (7.7)	98 (14.8)	0 (0.0)	383 (67.9)	309 (80.5)
UC San Diego CTIPM	3 (0.5)	386 (61.4)	258 (38.9)	647 (72.0)	0 (0.0)	0 (0.0)
Harvard University's Massachusetts General Hospital (MGH)	0 (0.0)	25 (4.0)	38 (5.7)	0 (0.0)	25 (4.4)	38 (9.9)
University of Rochester Medical Center (URMC)	0 (0.0)	18 (2.9)	233 (35.1)	251 (28.0)	0 (0.0)	0 (0.0)
UC San Francisco (UCSF)	0 (0.0)	22 (3.5)	20 (3.0)	0 (0.0)	22 (3.9)	20 (5.2)
UT Health Sciences Center San Antonio (UTHSCSA)	0 (0.0)	129 (20.5)	17 (2.5)	0 (0.0)	129 (22.9)	17 (4.4)
University of Cambridge	5 (0.9)	0 (0.0)	0 (0.0)	0 (0.0)	5 (0.9)	0 (0.0)
Manufacturer/Model						
GE Healthcare/Discovery MR750	554 (100.0)	278 (44.3)	189 (28.5)	470 (52.3)	340 (60.3)	211 (55.0)
GE Healthcare/Signa Premier	0 (0.0)	203 (32.3)	225 (33.9)	177 (19.7)	95 (16.8)	156 (40.6)
SIEMENS Healthcare/Magnetom Skyra	0 (0.0)	59 (9.4)	250 (37.6)	251 (28.0)	41 (7.3)	17 (4.4)
SIEMENS Healthcare/Magnetom Trio	0 (0.0)	88 (14.0)	0 (0.0)	0 (0.0)	88 (15.6)	0 (0.0)
Biopsy						
Biopsy-confirmed cases	322 (58.1)	361 (57.5)	664 (100.0)	689 (76.7)	274 (48.6)	384 (100.0)
Biopsy-naïve cases	400 (72.2)	164 (26.1)	664 (100.0)	613 (68.3)	231 (41.0)	384 (100.0)
Gleason Grade Group						
Benign	72 (13.0)	80 (12.7)	179 (27.0)	186 (20.7)	66 (11.7)	79 (20.6)
1	58 (10.5)	97 (15.5)	140 (21.1)	127 (14.1)	92 (16.3)	76 (19.8)
2	85 (15.3)	88 (14.0)	181 (27.3)	189 (21.0)	65 (11.5)	100 (26.0)
3	56 (10.1)	54 (8.6)	90 (13.6)	104 (11.6)	23 (4.1)	73 (19.0)
4-5	51 (9.2%)	42 (6.7)	74 (11.0)	83 (9.3)	28 (5.0)	56 (14.6)
PI-RADS score						
1	255 (46.0)	320 (51.0)	60 (9.0)	261 (29.1)	342 (60.6)	32 (8.3)
2	17 (3.1)	24 (3.8)	12 (1.8)	29 (3.2)	22 (3.9)	2 (0.5)
3	46 (8.3)	62 (9.9)	155 (23.3)	157 (17.5)	52 (8.2)	54 (14.1)
4	120 (21.7)	118 (18.8)	215 (32.4)	208 (23.1)	88 (15.6)	157 (40.9)
5	116 (20.9)	104 (16.5)	222 (33.5)	243 (27.1)	60 (10.7)	139 (36.2)

Table 1. Patient Demographic Characteristics in the Data Sets from Data Split 1 and Data Split 2. Unless otherwise specified, data are numbers of examinations, with percentages in parentheses. *The training set for Data Split 1 were acquired with the same RSI protocol. **Data are median with IQR in parentheses. csPCa = Clinically Significant Cancer (Gleason Grade Group ≥ 2 or PI-RADS ≥ 3). non-csPCa = Not having Clinically Significant Cancer (Benign, Gleason Grade Group = 1 or PI-RADS < 3 with a prostate-specific antigen density < 0.15). CTIPM = Center for Translational Imaging and Precision Medicine. UC = University of California. UT = University of Texas. PI-RADS = Prostate Imaging Reporting & Data System.

	1: PI-RADS	2: RSIRs-max	3: AI bpMRI	4: AI bpMRI-seg	5: AI bpMRI-seg + RSIRs-max	6: AI bpMRI-seg + RSI-seg + RSIRs-max	7: PI-RADS + RSIRs-max	8: PI-RADS + AI bpMRI-seg + RSIRs-max + RSI-seg
Detected vs. non-csPCa	Median (95% CI)	Median (95% CI)	Median (95% CI)	Median (95% CI)	Median (95% CI)	Median (95% CI)	Median (95% CI)	Median (95% CI)
A: GG≥2	0.74 (0.70-0.77)	0.72 (0.68-0.76)	0.68 (0.64-0.72)	0.72 (0.69-0.76)	0.72 (0.68-0.76)	0.73 (0.69-0.77)	0.77 (0.73-0.81)*	0.78 (0.74-0.81)*
B: GG2	0.69 (0.64-0.73)	0.69 (0.64-0.74)	0.62 (0.57-0.66)	0.70 (0.66-0.75)	0.70 (0.65-0.74)	0.68 (0.63-0.73)	0.73 (0.68-0.77)	0.72 (0.67-0.77)
C: GG3	0.74 (0.69-0.79)	0.72 (0.66-0.78)	0.72 (0.65-0.78)	0.71 (0.65-0.77)	0.70 (0.63-0.76)	0.74 (0.68-0.80)	0.78 (0.72-0.83)	0.79 (0.73-0.84)
D: GG4-5	0.85 (0.80-0.89)	0.80 (0.73-0.86)	0.78 (0.72-0.84)	0.79 (0.73-0.85)	0.81 (0.74-0.86)	0.85 (0.80-0.90)	0.87 (0.82-0.92)	0.90 (0.85-0.94)

Table 2. AUCs Results for Data Split 1. 95% CI refers to the 95 percent confidence interval. * refers to $p < 0.05$ for comparison of AUC vs. PI-RADS 1 (only reported for primary analysis, GG≥2). Model 1 refers to the logistic regression model with PI-RADS input; Model 2 refers to the logistic regression model with RSIRs-max input; Model 3 refers to the 3D DenseNet with T2w, ADC and high-b DWI input (bpMRI); Model 4 refers to the the 3D-DenseNet with T2w-seg, ADC-seg and high-b DWI-seg input (bpMRI-seg); Model 5 refers to the 3D-DenseNet+RSI with bpMRI-seg and RSIRs-max input; Model 6 refers to the 3D-DenseNet+RSI with bpMRI-seg, RSI-C₁-seg, RSI-C₂-seg (RSI-seg) and RSIRs-max input; Model 7 refers to the logistic regression model with PI-RADS and RSIRs-max input; Model 8 refers to the logistic regression model with PI-RADS and the output probability of Model 6. Group A) All the patients that are biopsy-naïve at time of MRI with biopsy confirmed diagnosis that are not used for training vs. non-csPCa (n=664). Group B) Subsets of Group A) with either GG2 csPCa and non-csPCa (n=500). Group C) Subsets of Group A) with either GG3 csPCa and non-csPCa (n=409). Group D) Subsets of Group A) with either GG4-5 csPCa and non-csPCa (n=393). n is the number of cases in each testing group.

	1: PI-RADS	2: RSIRs-max	6: AI bpMRI-seg + RSI-seg+ RSIRs-max	7: PI-RADS + RSIRs-max	8: PI-RADS + AI bpMRI-seg + RSIRs-max + RSI-seg
Detected vs. non-csPCa	Median (95% CI)	Median (95% CI)	Median (95% CI)	Median (95% CI)	Median (95% CI)
A: GG≥2	0.73 (0.68-0.78)	0.75 (0.70-0.80)	0.78 (0.73-0.83)	0.79 (0.74-0.83)*	0.81 (0.76-0.85)*
B: GG2	0.69 (0.63-0.75)	0.72 (0.66-0.75)	0.73 (0.66-0.79)	0.75 (0.69-0.81)	0.76 (0.70-0.82)
C: GG3	0.74 (0.67-0.80)	0.75 (0.68-0.82)	0.8 (0.73-0.86)	0.8 (0.73-0.86)	0.82 (0.75-0.88)
D: GG4-5	0.80 (0.74-0.86)	0.80 (0.72-0.87)	0.86 (0.80-0.92)	0.85 (0.79-0.91)	0.89 (0.83-0.94)

Table 3. AUCs Results for Data Split 2. Same as the setting of Table 2. 95% CI refers to the 95 percent confidence interval. * refers to $P < .05$ for comparison of AUC vs. PI-RADS 1 (only reported for primary analysis, GG≥2). Model 1 refers to the logistic regression model with PI-RADS input; Model 2 refers to the logistic regression model with RSIRs-max input; Model 6 refers to the 3D-DenseNet+RSI with bpMRI-seg, RSI-seg and RSIRs-max input; Model 7 refers to the logistic regression model with PI-RADS and RSIRs-max input; Model 8 refers to the logistic regression model with PI-RADS and the output probability of Model 6. Group E) All the patients that are biopsy-naïve at time of MRI with biopsy confirmed diagnosis that are not used for training vs. non-csPCa (n=384). Group F) Subsets of Group E) with either GG2 csPCa and non-csPCa (n=255). Group G) is subset of Group E) with either GG3 csPCa and non-csPCa (n=228). Group H) is subset of Group E) with either GG4-5 csPCa and non-csPCa (n=211). n is the number of cases in each testing group.